THE JOURNAL OF PHYSICAL CHEMISTRY C

pubs.acs.org/JPCC Article

Bonding Properties of Isolated Metal Atoms on Two-Dimensional Oxides

Published as part of The Journal of Physical Chemistry virtual special issue "Metal Clusters, Nanoparticles, and the Physical Chemistry of Catalysis".

Sergio Tosoni* and Gianfranco Pacchioni

Cite This: https://dx.doi.org/10.1021/acs.jpcc.0c05958 Read Online

ABSTRACT: We report a systematic comparative dispersion-corrected DFT study of single (K, Au, and Pt) atom adsorption over a wide range of metal-supported oxide ultrathin films (MgO on Ag and Mo, ZnO on Cu, Ag, and Au, SiO_2 on Pt and Ru, TiO_2 on Ag and Pt, and ZrO_2 on Pt and ZrPt). These films include reducible and non-reducible oxides and have been prepared and characterized experimentally, showing very unusual and interesting behavior toward metal atom adsorption. The interaction of K and Au with the metal/oxide substrates is dominated by charge-transfer aspects, where K tends to assume positive charge and Au negative charge. This fact reflects into a general trend where metal-supported oxide films displaying a large work function (i.e., deep empty states) tend to bind K cations strongly, while supports with small work function (i.e., shallow donor states) strongly stabilize Au in anionic form. The correlation between adsorption energy and work function is not strong enough to neglect several other aspects related to chemical and morphological properties of the specific oxide/metal interface. The case of Pt is completely different: here, covalent contributions to the bonding prevail, and the bond strength depends on factors such as the surface morphology and local atomic coordination, rather than the support's work function.

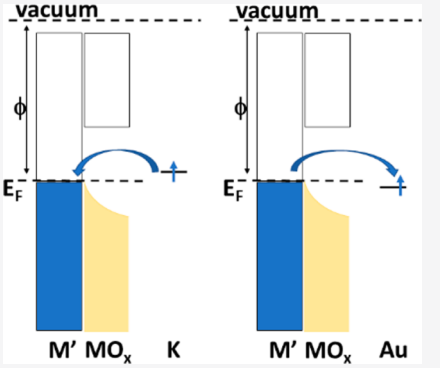

1. INTRODUCTION

Thin and ultrathin oxide films were first grown on metal supports with the aim to enable the study of the surface morphology with high-resolution electron microscopy techniques, whose usage on insulating bulk oxides is prevented by the large band gap.[1−4] However, metal-supported oxide two-dimensional films soon emerged as a new, interesting class of materials, whose properties depend on the low dimensionality of the film, as well as the interplay with the metal substrate.[5] This led to various applications of these films, for instance, as sensors,[6] as adsorbants,[7] or in electronics.[8]

A very interesting field where this type of films can be applied is heterogeneous catalysis.[9] Here, the metal-supported oxide thin films display a property which their bulk equivalents do not have, namely, the possibility to trigger the electron transfer from the metal substrate to a reactive adsorbate (or vice versa) via tunnelling through the film. This mechanism was first theoretically predicted for the case of the formation of a gold anion, Au^-, upon adsorption of a single gold adatom on magnesium oxide films with thickness spanning from one monolayer (ML) to three layers supported on molybdenum or silver.[10] The formation of the Au^- species causes a strong increase in the adsorption energy compared to the case of bulk MgO, where the adatom remains neutral.[11] Another unambiguous sign of the charge transfer is represented by the quenching of the magnetic moment of the Au atom, whose electronic configuration changes from ($5d^{10}6s^1$) to ($5d^{10}6s^2$) upon reduction to Au^-.[10] Later on, scanning tunnelling microscopy (STM) measurements confirmed that, in the presence of Au adatoms dispersed on the MgO bilayer/Mo(100) system, charge transfer indeed takes place, but the effect decreases with the film thickness and vanishes above 10−15 layers, in full agreement with the proposed electron tunnelling model.[12] Charge transfer via tunnelling through a MgO thin film supported on Mo or Ag was observed also in the case of molecular adsorbates such as O_2,[13] NO_2,[14,15] or CO_2 (only in the case of MgO ML on Mo),[16] as well as in the case of larger gold aggregates.[17,18] Interestingly, the negatively charged Au species show in turn high activity in environmentally strategic chemical reactions, such as the CO_2 upgrade to C2 products.[19] Also, the energy of the frontier orbitals of molecules adsorbed on

Received: June 30, 2020
Revised: August 18, 2020
Published: September 1, 2020

metal-supported MgO films can be, to some extent, tuned depending on the film's thickness.[20] In general, the factors controlling the electron transfer have been recently carefully analyzed based on new experimental observations.[21]

The activation of atoms, molecules, and aggregates triggered by electron tunnelling from a metal support through an oxide thin film is not restricted to the special case of MgO supported on Ag or Mo. On the contrary, it has been recently shown that the active phase in catalytic methanol synthesis over the commercially used $Cu/ZnO/Al_2O_3$ ternary catalyst consists of a thin ZnO layer grafted on the copper particles.[22,23] A detailed characterization of a ZnO thin film growth on Cu(111) revealed that the film is a bilayer whose structure is a flat, nonpolar graphitic-like hexagonal arrangement, thus radically differing from the most stable ZnO bulk structure, wurtzite.[24] The role of interplay with the metal support in tuning the charge transfer at the ZnO surface has been studied computationally by simulating the adsorption of a probe molecule, CO, on the ZnO graphitic bilayer supported on the whole series of coinage metals (Cu, Ag, Au).[25] Charge transfer to electronegative adsorbates was shown to be related to the support's work function, following a trend where Cu is more prone to donate electrons than Ag, which is in turn more reactive than Au. Overall, the transformation of a single Au adatom to Au^- was predicted on ZnO supported on all three coinage metals based on DFT calculations.[26] A similar charge transfer was found for NO_2 and O_2 on ZnO/Cu only, while NO and CO_2 did not show any remarkable activation related to the charge transfer.[26] Similar to what was reported for MgO/Mo and MgO/Ag, also in the case of ZnO/Cu, the charge transfer takes place in the presence of gold adducts much larger than the single atom.[27]

In an attempt to rationalize and generalize the findings summarized above, one can recall that the electron tunnelling effect through a dielectric film in the nanometric (or sub-nanometric) thickness regime is regulated by two main factors: (i) the film thickness and (ii) the reciprocal alignment of the electronic levels of the involved species. On the latter aspect, what counts is the relative energy of the adsorbate's frontier orbitals with respect to the metal's Fermi energy: if the LUMO lies below the Fermi energy, an electron from the metal may flow through the film forming an anion. On the contrary, a HOMO orbital located above the Fermi level would lead to the formation of a cation.[5]

Beside MgO and ZnO, other oxides have been prepared in recent years in the form of ultrathin films, where the thickness of the film is typically 1−2 atomic layers. These include silica, titania, and zirconia. Some of these oxides belong to the class of wide gap, non-reducible oxides (silica and zirconia); others are classical reducible oxides (titania). A comparative study of their adsorption properties is thus relevant also in order to assess the changes in the properties of oxide materials as their dimensionality is reduced via nanostructuring.

The aim of this paper is to provide a systematic report on the adsorption of single adatoms on a wide series of metal-supported oxide films, discussing the related charge transfer phenomena. Some of the systems discussed in this paper have been studied before. However, this is the first attempt to (i) create a large database of systems treated on the same footing using the same level of theory and (ii) identify a quantitative correlation between the adsorption strength and some physicochemical descriptors of the metal/oxide interface. To this end, we extend the case of the Au single atoms discussed above, and we parallelly explore the adsorption of an alkaline earth metal, namely, K. This permits one to study the electron transfer in both directions, from the metal to the adatom in the case of the more electronegative adsorbate (Au) and from the adatom to the metal substrate in the case of K. We also extend the case to another transition metal single atom, Pt, more prone to form covalent interactions on surfaces. It is worth remembering that the adsorption and stabilization of single adatoms on oxidic substrates is a topic whose relevance goes beyond the proof of concept on the charge transfer and electron tunnelling hereby described. On the contrary, single metal atoms stabilized on oxidic or carbon-based supports are seen as the ultimate form of dispersed catalytically active metal particles in heterogeneous catalysis, the so-called single atom catalyst.[28−32] Similarly, the magnetic properties of transition metal and rare earth single atoms supported on MgO/Ag have been intensively studied, representing, in principle, the smallest possible switchable memory device.[33−37]

As for the oxide/metal substrates, the present study includes, beyond the aforementioned structures (MgO ML and BL supported on Ag(100) and Mo(100)[16,37−39] and ZnO BL supported on (111) coinage metal surfaces[25]), other systems that we have already characterized in the past: the SiO_2 BL supported on Pt(111) and Ru(0001),[40] the TiO_2 lepidocrocite BL on Pt(111) and Ag(100),[41] and the ZrO_2 ML supported on Pt(111) and on a ZrPt alloy.[42]

The topic of the adsorption of adatoms on metal-supported thin films has been the object of previous experimental and computational investigations. Such is the case of the adsorption of alkali metal[43] and transition metal (Pd, Ag, and Au adatoms)[10,11] on MgO/Mo, alkali (Li, Na, K)[44] and transition metal atoms (Au, Pd)[45] on $(SiO_2)_{BL}/Ru$, and transition metal adatoms (Au, Ag, Pd, Ni, Fe) on $(ZrO_2)_{ML}/ZrPt$.[46] The novelty of the present paper relies on its systematic character, allowing one to relate trends in an adatom's oxidation state and adsorption energy to the physicochemical properties of the metal/oxide interface.

This work is organized as follows: In section 2, the general methodology is exposed. For the specific computational details on each system, the reader is addressed to the Supporting Information. In section 3, we report a detailed description of K, Au, and Pt adsorption on each surface. For simplicity, only the most stable configuration is discussed. A complete list of all local minima is included in the Supporting Information. Section 4 is dedicated to the general discussion and conclusive remarks.

2. COMPUTATIONAL METHODS

All calculations have been performed with the plane-wave code VASP.[47,48] The core electrons are treated with the projector augmented wave method,[49,50] and the external electrons are represented by a set of plane waves expanded within a kinetic energy cutoff of 400 eV. A list of pseudopotentials adopted for all atomic species is reported in the Supporting Information, Table S1. We adopt the generalized gradient approximation of the density functional theory, as formulated in the Perdue−Burke−Ernzerhof (PBE) functional.[51] The general tendency toward the underestimation of the oxides' band gap by the GGA functionals is hereby handled by including the on-site Coulomb interaction as in the Hubbard model (GGA+U)[52,53] on metal cations in the oxide films with a strong correlation character. Based on evidence discussed in previous works, a U parameter of 3 eV is used for Ti(3d) orbitals in TiO_2,[41] U = 4 eV for Zr(4d) in ZrO_2,[42] and U = 4.7 eV for Zn(3d) in ZnO.[25] The choice of the U parameter is delicate, as it may remarkably influence the extent

https://dx.doi.org/10.1021/acs.jpcc.0c05958
J. Phys. Chem. C XXXX, XXX, XXX−XXX

Table 1. K, Pt, and Au Adsorption on Free-Standing and (Ag, Mo)-Supported MgO Mono- and Bilayer[a]

atom	support	φ (eV)	site	D_e (eV)	M (|e|)	q_A (|e|)	O.S.	R_O (Å)	R_{Mg} (Å)
K	MgO-free		O-top	−0.28	1.00	+0.30	0	2.88	3.71
	MgO_{ML}/Ag	3.29	hollow	−1.26	0.00	+0.82	+1	2.67	3.16
	MgO_{BL}/Ag	2.91	hollow	−0.66	0.00	+0.82	+1	2.69	3.10
	MgO_{ML}/Mo	2.5	hollow	−0.50	0.00	+0.57	0	2.89	3.27
	MgO_{BL}/Mo	2.04	O-top	−0.50	0.43	+0.32	0	2.83	3.71
Pt	MgO-free		O-top	−2.55	0.04	−0.35	0	1.97	2.92
	MgO_{ML}/Ag	3.29	O-top	−2.85	0.00	−0.69	−1	2.10	2.82
	MgO_{BL}/Ag	2.91	O-top	−2.58	0.49	−0.66	−1	2.07	2.86
	MgO_{ML}/Mo	2.5	hollow	−4.09	0.08	−1.31	−2	3.14	2.55
	MgO_{BL}/Mo	2.04	O-top	−3.65	0.95	−0.96	−1	2.20	2.89
Au	MgO-free		O-top	−1.09	1.00	−0.29	0	2.26	3.13
	MgO_{ML}/Ag	3.29	O-top	−1.99	0.00	−0.77	−1	2.76	3.07
	MgO_{BL}/Ag	2.91	hollow	−1.82	0.00	−0.84	−1	3.20	2.83
	MgO_{ML}/Mo	2.5	hollow	−3.17	0.00	−0.81	−1	3.10	2.75
	MgO_{BL}/Mo	2.04	hollow	−2.84	0.02	−0.84	−1	3.14	2.81

[a]Film−metal work function (φ, eV), preferential adsorption site, adsorption energy (D_e, eV), magnetic moment (M, |e|), and Bader charge (q_A, |e|) and estimated formal oxidation state (O.S.) of the adsorbed adatom, minimum adatom−oxygen (R_O, Å), and adatom−magnesium (R_{Mg}, Å) bond distances.

of the charge transfer.[54] However, for all of the aforementioned oxides, the U value has been carefully assessed in our previous works.

A critical aspect in the occurrence of a charge transfer between an adsorbed atom and the metal support via electron tunnelling through a thin insulating film is the band alignment of the energy levels of the various components. These depend on the level of treatment, and DFT+U represents only an approximate way to solve the problem of the self-interaction correction. This problem has been systematically addressed for the case of FeO/Pt[55] and MgO/Ag[56] with the general outcome that, while the absolute values of the quantities calculated, in particular the energetics, depend to some extent on the method used, the occurrence of the charge transfer is independent of the level of treatment.

The long-range dispersion forces are added according to the two-body semiempirical method (DFT+D2) originally proposed by Grimme,[57] where the C6 and R0 parameters of the metal cations in the oxides are rescaled accounting for their partial ionic character.[58] This scheme (DFT+D2′) improves the description of adsorption phenomena on ionic oxide surfaces with respect to the original D2 but also leads to metal−oxide interfacial properties similar to those obtained with the less empirical van der Waals functionals, as proven for the paradigmatic case of MgO/Ag.[37,56]

The magnetic moment of the adsorbed adatoms is determined recurring to spin-polarized calculations. Dipole corrections to the energy are applied along the nonperiodic direction of the cell. Atomic charges are evaluated according to the model proposed by Bader.[59,60] Model structures for metal-supported thin films are constructed minimizing the strain arising from the lattice mismatch, which is then released on the film. In some cases, it is necessary to recur to rather large supercells; this, in turn, ensures that the adsorption of adatoms is simulated at small concentration. In the case of very favorable metal−oxide epitaxial match, leading to small metal−oxide supercells, the lateral adatom−adatom interactions may play a role. For the comparative sake of this paper, we always ensure a minimum distance between nearby adsorbates of 9.8 Å, conveniently expanding the metal−oxide cell when necessary. A complete list of all adopted reconstructions and supercells is reported in the Supporting Information, Table S2.

All surfaces are treated with periodically repeated slab models, and a vacuum layer of at least 15 Å thickness is included in the cell to avoid spurious interactions between replicas.

The adsorption energy, D_e, is calculated as in eq 1

$$D_e = E(A/MO_x/M') - E(MO_x/M') - E(A) \quad (1)$$

where A is the (K, Pt, Au) adatom, MO_x is the oxide thin film, and M′ is the metal support. The reference energy for each adatom is calculated as the energy of the atom in the gas phase in its fundamental electronic state. A complete exploration of the potential energy surface has not been performed, and the adatom's adsorption site is determined as the minimum energy state among several structures obtained by static relaxations. A comprehensive list of all local minima is available in the Supporting Information.

3. RESULTS

3.1. MgO Mono- and Bilayer Supported on Ag and Mo.

In the case of MgO, we compare the adsorption on a free-standing four-layer slab (whose surface properties are well converged with respect to the thickness) to mono- and bilayers supported on Ag and Mo, thus considering both the effect of the support and the thickness on the film's adsorptive properties. On free-standing MgO, K is weakly physisorbed (D_e = −0.28 eV) in an O-top position, Table 1 and Figure 1. Given the irreducible nature of MgO, even an alkali metal with a small ionization energy such as K maintains its neutral state upon adsorption, as shown by the adatom's doublet spin state (M = 1.00). The bonding mode of K to MgO surfaces has been fully characterized by combining DFT calculations with electron paramagnetic resonance (EPR) measurements.[61] The present result is in agreement with previous reports,[43] even though the hereby reported D_e is slightly larger compared to the literature, due to the inclusion of the dispersion forces in the present work. On metal-supported MgO films, the substrate's work function decreases going from 4.25 eV in Ag(100) and 3.84 eV in Mo(100) to 3.29 eV (MgO_{ML}/Ag), 2.91 eV (MgO_{BL}/Ag), 2.50 eV (MgO_{ML}/Mo), and 2.04 eV (MgO_{BL}/Mo). A larger work function implies the presence of a deeper acceptor state at the

https://dx.doi.org/10.1021/acs.jpcc.0c05958
J. Phys. Chem. C XXXX, XXX, XXX−XXX

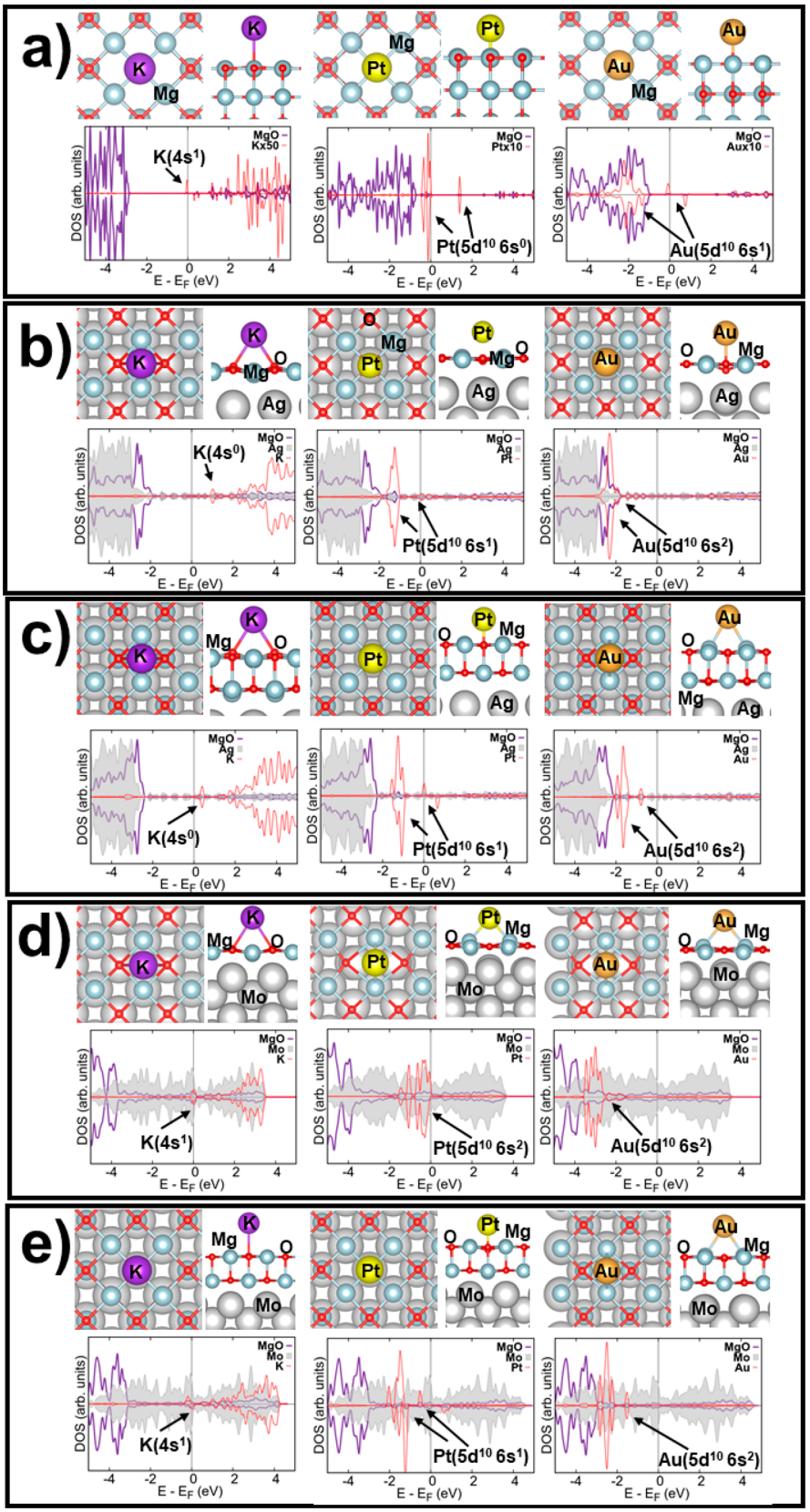

Figure 1. Top view, side view, and PDOS plot of K (left), Pt (middle), and Au (right) adatoms adsorbed on (a) free-standing MgO, (b) MgO_{ML}/Ag, (c) MgO_{BL}/Ag, (d) MgO_{ML}/Mo, and (e) MgO_{BL}/Mo.

metal's Fermi level, which should favor a charge transfer from the K adatom. This is indeed the case for both ML and BL supported on Ag: the K adatom moves to a hollow site and acquires null magnetization, and an electron is transferred from K (4s) to the metal substrate, as one can see from the projected DOS reported in Figure 1c. The adsorption energy, D_e, follows

https://dx.doi.org/10.1021/acs.jpcc.0c05958
J. Phys. Chem. C XXXX, XXX, XXX−XXX

Table 2. K, Pt, and Au Adsorption on Free-Standing and (Cu, Ag, Au)-Supported ZnO Bilayer[a]

atom	support	φ (eV)	site	D_e (eV)	M (|e|)	q_A (|e|)	O.S.	R_O (Å)	R_{Zn} (Å)
K	ZnO-free		hollow	−1.93	0.00	+0.84	+1	2.71	3.17
	ZnO/Cu	4.16	hollow	−2.62	0.00	+0.86	+1	2.71	3.14
	ZnO/Ag	4.32	hollow	−2.80	0.00	+0.88	+1	2.73	3.19
	ZnO/Au	4.96	hollow	−3.33	0.00	+0.88	+1	2.73	3.20
Pt	ZnO-free		O(top)	−2.51	0.02	−0.15	0	1.98	2.57
	ZnO/Cu	4.16	O(top)	−2.69	0.48	−0.42	−1	2.31	2.53
	ZnO/Ag	4.32	hollow	−3.06	0.00	−0.71	−2	3.23	2.49
	ZnO/Au	4.96	O(top)	−2.54	0.00	−0.10	0	1.98	2.57
Au[b]	ZnO-free		bridge	−0.87	1.00	−0.11	0	2.59	2.33
	ZnO/Cu	4.16	hollow	−2.10	0.00	−0.46	−1	3.16	2.67
	ZnO/Ag	4.32	hollow	−2.20	0.00	−0.47	−1	3.16	2.67
	ZnO/Au	4.96	hollow	−1.73	0.00	−0.46	−1	3.18	2.66

[a]Film−metal work function (φ, eV), preferential adsorption site, adsorption energy (D_e, eV), magnetic moment (M, |e|), and Bader charge (q_A, |e|) and estimated formal oxidation state of the adsorbed adatom (O.S.), minimum adatom−oxygen (R_O, Å) and adatom−zinc (R_{Zn}, Å) bond distances. [b]Data from ref 26.

the trend of the substrate's work function and becomes −1.26 eV (MgO_{ML}/Ag) and −0.66 eV (MgO_{BL}/Ag). For Mo-supported films, in the case of the ML, the K adatom is bound on a hollow site (as for MgO/Ag) with an adsorption energy of −0.50 eV. For MgO_{BL}/Mo, the most favorable site is O-top, just like in the case of free-standing MgO, and D_e is −0.50 eV. The oxidation state of the K adatom can be discussed based on the projected DOS reported in Figure 1d and e. In the case of MgO_{BL}/Mo, the K(4s) orbital is singly occupied (the magnetization on the adatom is 0.43 |e|). In the case of MgO_{ML}/Mo, the K(4s) state lies across the Fermi level and the orbital is singly occupied but with a spin-contaminated half-α/half-β character: an actual charge transfer, thus, does not take place. The supporting metal plays therefore a major role in determining the adatom's oxidation state, since a charge transfer takes place on MgO/Ag, while K remains basically neutral on MgO/Mo.

Also, in the case of Pt, the most favorable adsorption site and the adatom's oxidation state vary due to the interplay between the film's thickness and the metal's support. On free-standing MgO, Pt is adsorbed on the O-top position, but at variance from K, the adsorption energy is large (D_e = −2.55 eV). This indicates that a strong covalent interaction takes place. On metal-supported films, the actual oxidation state of the adatom as well as the adsorption site and energy depend on the film thickness and support work function. On MgO_{BL}/Ag, Pt is adsorbed on an O-top site with a D_e of −2.58 eV, in close similarity to the free-standing case. However, the Pt(6s) orbital is partly occupied, as shown by the adatom's magnetization (0.49 |e|) and the p-DOS plot in Figure 1c. The adatom has thus acquired a charge of −1. A similar oxidation state and adsorption geometry is reported on MgO_{ML}/Ag, but here, D_e is larger (−2.85 eV). In this case, however, the electron in the Pt(6s) orbital has half alpha−half beta character, so no net magnetization is reported.

The picture is quite different on Mo-supported films, where the smaller work function enables a charge transfer from the metal substrate to the adatom, forming a Pt^- species (BL) and Pt^{2-} species (ML). The charge transfer implies also a strong increase (in absolute value) in D_e, which becomes −4.09 eV for ML and −3.65 eV for BL.

In the case of Au, the adatom maintains a neutral state only on free-standing MgO, with a D_e of −1.09 eV. The most favorable adsorption site is O-top. This result is very similar to a previous report.[11] On Ag- and Mo-supported films, an anion is always formed, as is evident from the null magnetization of the Au adatom. On MgO_{ML}/Ag, D_e is equal to −1.99 eV and the adatom is on the O-top site (in a previous report, the O-top site was found to be 0.04 eV less stable than the hollow one[35]). In the case of MgO_{BL}/Ag, D_e reduces to −1.82 eV and the adatom moves to a hollow site. On Mo, the removal of an electron from the substrate is easier, and this translates into a larger D_e, which is now −3.17 eV for ML and −2.84 eV for BL. On both MgO_{BL}/Mo and MgO_{BL}/Mo, Au is preferentially adsorbed on a hollow site. In a previous report, the most favorable adsorption site was found to be Mg-top and also the adsorption energy was for both ML and BL in the range −2.2/−2.3 eV.[11] In that case, however, a C_{4v} symmetry constraint was enforced, thus ruling out the hollow position as a possible adsorption site, and the long-range dispersion was not included. The trend in Au adsorption energy, however, cannot be predicted only based on the work function argument: indeed, for both Ag and Mo, the work function for the supported ML is larger than that for BL. One may thus expect that the Au anion binds stronger on supported BL compared to ML, while the opposite is found. A possible explanation relies on Coulombic factors hindering the charge separation between negatively charged adatoms and metal support, favoring the ML case, where the distance between negative adatom and positive metal support is smaller. The overlap between orbitals from the adatom and the metal surface, which can also contribute in stabilizing the adatom, is also larger in the case of supported MLs compared to BLs.

3.2. ZnO Graphitic Bilayer Supported on Coinage Metals. The adsorption of a K single atom on free-standing and metal-supported ZnO bilayer leads, in all cases, to the ionization of the adatom to K^+, Table 2 and Figure 2. This is confirmed by the positive Bader charge and the complete quenching of the magnetic moment. In all cases, the most favorable adsorption site is the hexagonal hollow (Figure 2), and both K−O and K−Zn distances are hardly affected by the support. Notably, the adsorption energy, D_e, varies significantly, passing from −1.93 eV for free-standing ZnO to −2.62 eV for ZnO/Cu, −2.80 eV for ZnO Ag, and −3.33 eV for ZnO/Au. In the case of free-standing ZnO, the electron goes to the ZnO conduction band, while, in the case of metal-supported films, the electron tunnels through the film and is captured by the metal support. The latter mechanism clearly stabilizes the adsorption of K adatoms. The larger the metal's work function, the larger the gain in adsorption energy with respect to the free-standing ZnO film, Table 2.

https://dx.doi.org/10.1021/acs.jpcc.0c05958
J. Phys. Chem. C XXXX, XXX, XXX−XXX

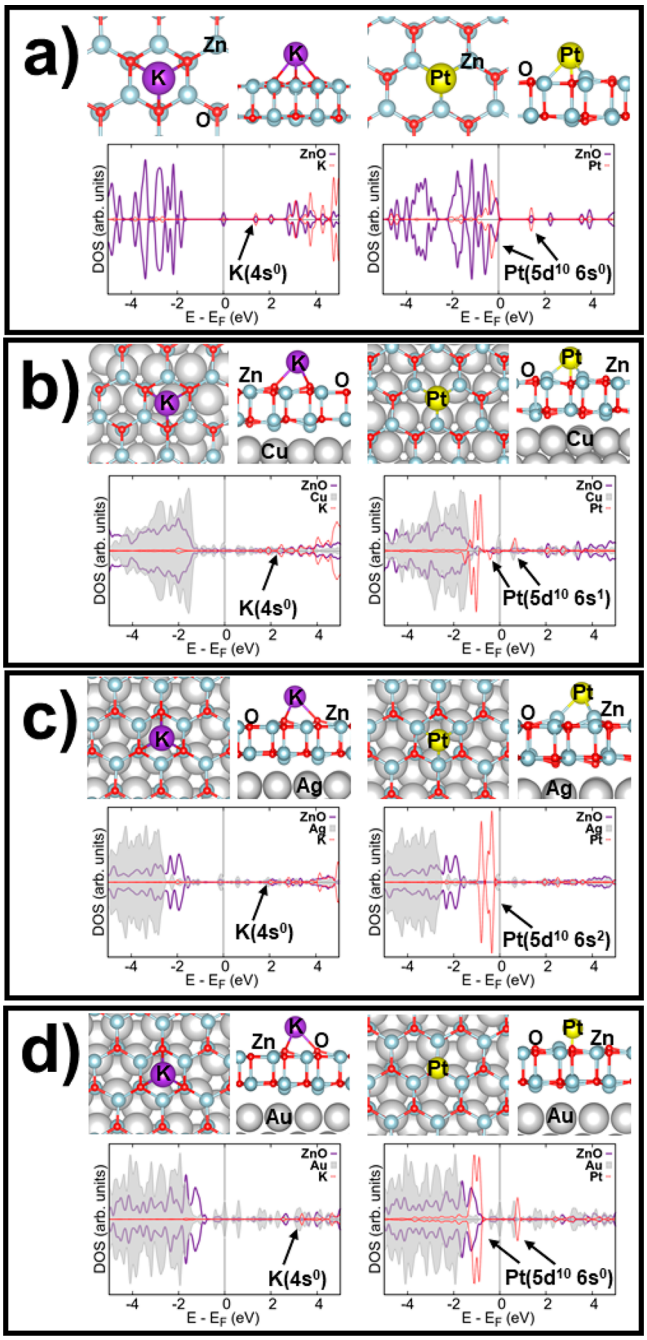

Figure 2. Top view, side view, and PDOS plot of K (left) and Pt (right) adatoms adsorbed on (a) free-standing ZnO, (b) ZnO_{BL}/Cu, (c) ZnO_{BL}/Ag, and (d) ZnO_{BL}/Au. Data on Au_1 adsorption are reported in ref 26.

The adsorption of Pt_1 species on ZnO/(Cu, Ag, Au) provides a more complex picture. On the free-standing ZnO BL, the Pt adatom is preferentially bound in an O-top configuration and maintains a neutral state. The complete quenching of the magnetic moment suggests a transition from a ($5d^9$, $6s^1$)- to a ($5d^{10}$, $6s^0$)-like electronic configuration. This fact together with the large adsorption energy (D_e = −2.51 eV) and the small negative Bader charge (−0.15 |e|) suggests that a covalent bond, with some polar character, is established between Pt and O, at a bond distance of 1.98 Å. The same kind of bonding, under all aspects, is observed for ZnO/Au. In the case of ZnO/Cu, the adatom is also bound on an O-top site, with a Zn−O distance of 2.31 Å, remarkably larger than on ZnO/Au (1.98 Å). The adsorption energy is −2.69 eV, and a residual magnetization (0.48 |e|) is present on the adatom, indicating a partial occupation of the Pt(6s) orbital. On ZnO/Ag, then, the hollow site results are more favorable than those of the O-top site, and the adsorption energy is −3.06 eV, the largest value in the series. The adatom is much closer to the Zn ions than to the O ones, and its Bader charge is −0.71 |e|, which definitely suggests that a remarkable charge transfer took place. If one looks at the PDOS for the adatom's states in Figure 2c, one can conclude that both the 5d and 6s orbitals are fully occupied and the Pt adatom is formally in a −2 oxidation state. In principle, a charge transfer from the Cu substrate should be more favorable compared to Ag, given its smaller work function. However, the more diffuse nature of Ag orbitals compared to Cu may be an important factor in determining the final oxidation state of the Pt adatom, due to the more efficient mixing of adatom's and substrate's states in the case of Ag.

In the case of Au_1 adsorption, we hereby include, for the sake of completeness, data obtained with the very same computational setup and previously published.[26] The oxidation state of the adatom is 0 on the free-standing film and switches to −1 on metal-supported ZnO. In this case, the assignment of the formal oxidation state can be immediately derived from the magnetization of the Au adatom, which maintains its $5d^{10}$ $6s^1$ doublet spin state on the free-standing film, while it switches to a singlet $5d^{10}$ $6s^2$ configuration on the metal-supported film. Notably, the Bader model is not unambiguous, attributing an anionic character to the Au adatom always considerably smaller than −1 (the charge is about −0.5 |e| for Cu-, Ag-, and Au-supported ZnO). While neutral Au is preferentially adsorbed on a ZnO bridge site, Au^- goes to a hollow site. The free-standing film binds the Au adatom weakly (−0.87 eV) compared to the metal-supported ones, where D_e is −2.10 on ZnO/Cu, −2.20 on ZnO/Ag, and −1.73 on ZnO/Au. The smaller D_e reported for ZnO/Au fits with the larger work function of Au compared to other coinage metals. Based on this argument, however, one would expect a slightly larger D_e for ZnO/Cu compared to ZnO/Ag, while the contrary is observed. This can be explained as an effect of the more protruding nature of Ag orbitals compared to Cu ones, contributing to stabilize adsorption of both Pt (vide supra) and Au adatoms on ZnO/Ag compared to ZnO/Cu. One should also mention that, as previously discussed, the structure of the ZnO film undergoes remarkable distortions when put in contact with Cu compared to more inert supports such as Ag or Au. Of course, this structural aspect may also play a role.

3.3. SiO_2 Bilayer Supported on Pt and Ru. The class of 2D vitreous materials growth on metals is wide and complex. Here, we focus on a simple structure, represented by a crystalline SiO_2 bilayer whose surface displays a regular arrangement of hexagonal rings. Si and O atoms are four- and two-coordinated, respectively, i.e., chemically saturated. We study K, Pt, and Au adsorption on the silica bilayer either free-standing or supported on Pt(111) and Ru(0001). The K atom is always ionized, as shown by the large and positive Bader charge and the quenching of its magnetic moment (Table 3), but its adsorption energy strongly depends on the support, spanning from −0.60 eV (free-standing SiO_2 in close agreement to a previous report[44]) to −1.27 eV (Ru-supported SiO_2) and −2.81 eV (on Pt-supported silica). The much larger D_e observed on SiO_2/Pt fits with its larger work function compared to SiO_2/Ru. In all cases, the K^+ cation is preferentially coordinated on a hollow site (Figure 3),

https://dx.doi.org/10.1021/acs.jpcc.0c05958
J. Phys. Chem. C XXXX, XXX, XXX−XXX

Table 3. K, Pt, and Au Adsorption on Free-Standing and (Pt, Ru)-Supported SiO_2 Bilayer[a]

atom	support	φ (eV)	site	D_e (eV)	M (|e|)	q_A (|e|)	O.S.	R_O (Å)	R_{Si} (Å)
K	SiO_2-free		hollow	−0.60	0.00	+0.77	+1	3.00	3.70
	SiO_2/Pt	4.97	hollow	−2.81	0.12	+0.89	+1	2.96	3.65
	SiO_2/Ru	3.67	hollow	−1.27	0.00	+0.91	+1	2.95	3.65
Pt	SiO_2-free		O-top	−0.50	0.09	−0.04	0	2.03	2.97
	SiO_2/Pt	4.97	bridge	−1.17	0.00	−0.10	0	1.99	2.39
	SiO_2/Ru	3.67	Si-top	−1.27	1.12	−0.47	−1	2.89	2.33
Au	SiO_2-free		hollow	−0.17	1.00	+0.02	0	3.39	4.06
	SiO_2/Pt	4.97	hollow	−0.12	1.00	+0.01	0	3.39	4.01
	SiO_2/Ru	3.67	Si-top	−1.25	0.00	−0.61	−1	2.95	2.41

[a]Film−metal work function (φ, eV), preferential adsorption site, adsorption energy (D_e, eV), magnetic moment (M, |e|), and Bader charge (q_A, |e|) and estimated formal oxidation of the adsorbed adatom, minimum adatom−oxygen (R_O, Å), and adatom−silicon (R_{Si}, Å) bond distances.

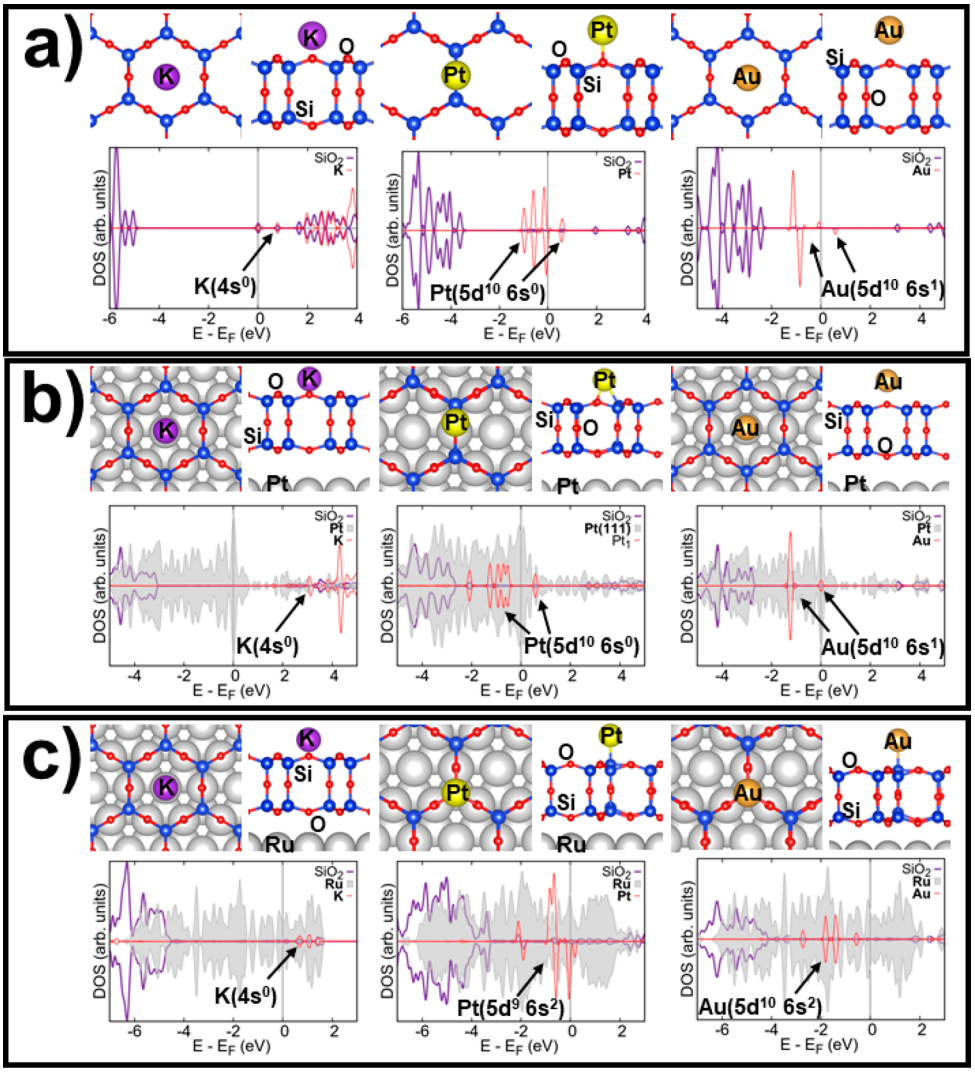

Figure 3. Top view, side view, and PDOS plot of K (left), Pt (middle), and Au (right) adatoms adsorbed on (a) free-standing SiO_2, (b) SiO_2/Pt, and (c) SiO_2/Ru.

with K−O distances close to 3.0 Å and K−Si distances around 3.7 Å.

The Pt atom maintains its neutral state on free-standing SiO_2 and SiO_2/Pt, while the more electropositive Ru support allows for the formation of a negatively charged Pt^- species. The most favorable adsorption site varies from O-top (free-standing silica) to bridge (SiO_2/Pt) and Si-top (SiO_2/Ru) depending on the support. On free-standing SiO_2, Pt is bound with an adsorption energy of −0.50 eV and a Pt−O distance of 2.03 Å. On SiO_2/Pt, the adsorption energy is −1.17 eV. The Pt−O distance is 1.99 Å, and the Pt−Si distance is 2.39 Å. In the case of SiO_2/Ru, finally, Pt is adsorbed in coincidence to a Si lattice site, with a Pt−O distance of 2.89 Å and a Pt−Si distance of 2.33 Å. The adsorption energy, −1.27 eV, is slightly larger than that on SiO_2/Pt.

https://dx.doi.org/10.1021/acs.jpcc.0c05958
J. Phys. Chem. C XXXX, XXX, XXX−XXX

Table 4. K, Pt, and Au Adsorption on Free-Standing and (Pt, Ag)-Supported TiO_2 Bilayer[a]

atom	support	φ (eV)	site	D_e (eV)	M (lel)	q_A (lel)	O.S.	R_O (Å)	R_{Ti} (Å)
K	TiO_2-free		O(4c)	−2.73	0.00	+0.91	+1	2.89	3.39
	TiO_2/Pt	5.33	Ti(up)	−3.42	0.00	+0.91	+1	2.79	3.37
	TiO_2/Ag	5.39	O(4c)	−2.86	0.00	+0.91	+1	2.85	3.46
Pt	TiO_2-free		Ti(down)	−3.21	0.05	+0.08	0	2.05	2.79
	TiO_2/Pt	5.33	Ti(down)	−4.06	0.00	+0.01	0	2.02	2.72
	TiO_2/Ag	5.39	Ti(down)	−3.64	0.01	+0.03	0	2.04	2.70
Au	TiO_2-free		O(4c)	−0.39	1.00	+0.10	0	2.88	3.08
	TiO_2/Pt	5.33	Ti(up)	−1.76	0.00	−0.30	−1	2.98	2.66
	TiO_2/Ag	5.39	O(4c)	−1.31	0.00	−0.26	−1	2.89	2.72

[a]Film−metal work function (φ, eV), preferential adsorption site, adsorption energy (D_e, eV), magnetic moment (M, lel), and Bader charge (q_A, lel) and estimated formal oxidation state of the adsorbed adatom, minimum adatom−oxygen (R_O, Å), and adatom−titanium (R_{Ti}, Å) bond distances.

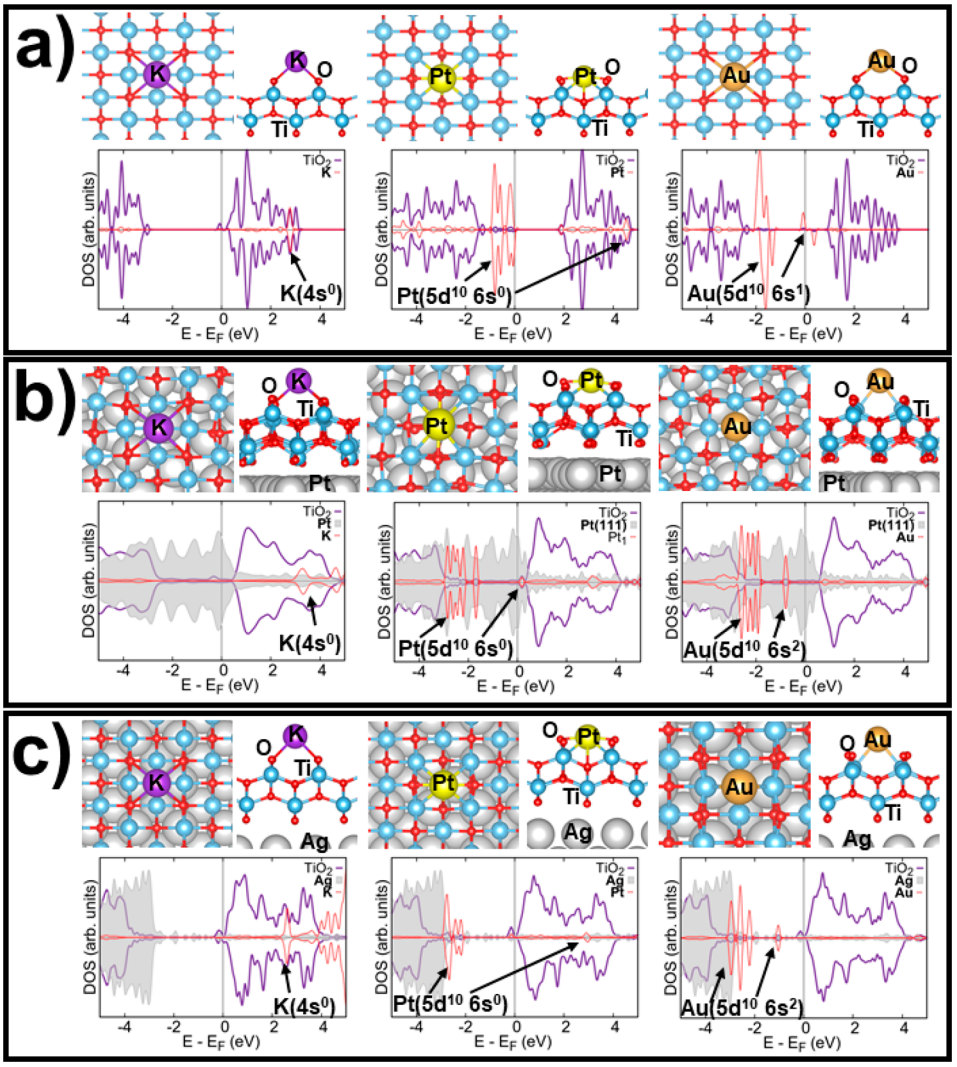

Figure 4. Top view, side view, and PDOS plot of K (left), Pt (middle), and Au (right) adatoms adsorbed on (a) free-standing TiO_2, (b) TiO_2/Pt, and (c) TiO_2/Ag.

In the case of Au, the adatom's oxidation state is determined by the support in strong analogy to the case of Pt. While Au maintains its neutral state on free-standing and Pt-supported silica, a Au^- anion is formed on SiO_2/Ru. This is shown by the Au magnetic moment (close to 1 for neutral Au and close to 0 for Au^-) and, at least qualitatively, also by the Bader charges. The electron transfer from the support to the adatom, in the case of SiO_2/Ru, increases the adsorption energy (−1.25 eV) by almost 1 eV compared to free-standing SiO_2 and SiO_2/Pt. The change of the oxidation state is also reflected in a change in adsorption site, which is hollow for neutral Au and Si-top for Au^-. Overall, this support-dependency of the Pt and Au oxidation state can be well explained: the adatoms maintain their neutral state on free-standing silica, as expected for such a scarcely basic oxide, while they can drag an electron from the Ru support, thanks to its smaller work function (3.67 eV) compared to Pt (4.97 eV).

https://dx.doi.org/10.1021/acs.jpcc.0c05958
J. Phys. Chem. C XXXX, XXX, XXX−XXX

Table 5. K, Pt, and Au Adsorption on Free-Standing and (Pt, ZrPt)-Supported ZrO_2 Monolayer[a]

atom	support	φ (eV)	site	D_e (eV)	M (lel)	q_A (lel)	charge	R_O (Å)	R_{Zr} (Å)
K	ZrO_2-free		Zr	−1.04	0.01	+0.89	+1	2.80	3.28
	ZrO_2−Pt	4.60	O(up)	−2.73	0.00	+0.88	+1	2.60	3.47
	ZrO_2−ZrPt	4.63	O(down)	−2.68	0.00	+0.89	+1	2.64	3.70
Pt	ZrO_2-free		O(up)	−2.04	0.07	−0.08	0	1.95	2.91
	ZrO_2−Pt	4.60	O(up)	−4.41	0.00	−0.09	0	2.06	2.68
	ZrO_2−ZrPt	4.63	O(down)	−3.47	0.00	−0.09	0	2.04	2.81
Au	ZrO_2-free		Zr	−0.44	0.41	−0.01	0	2.94	2.95
	ZrO_2−Pt	4.60	O(up)	−1.78	0.00	−0.58	−1	2.86	2.94
	ZrO_2−ZrPt	4.63	O(down)	−1.02	0.00	−0.57	−1	2.89	3.06

[a]Film−metal work function (φ, eV), preferential adsorption site, adsorption energy (D_e, eV), magnetic moment (M, lel), and Bader charge (q_A, lel) and estimated formal oxidation state of the adsorbed adatom, minimum adatom−oxygen (R_O, Å), and adatom−zirconium (R_{Zr}, Å) bond distances.

It must be stated that, in fact, given the porous nature of silica, adatoms may also be strongly bound at the metal/oxide interface, which can be reached by diffusion through the pore or at domain boundaries, at grain borders, or through larger rings present in amorphous domains. This has been shown in the case of Au adatoms on SiO_2/Ru or Li atoms on SiO_2/Mo(112) in joined experimental and computational works,[43,45] and also for Na^+ and Mg^{2+} cations in a computational study.[44] For the comparative sake of the present work, however, we do not investigate the penetration of adatoms through the oxide film to the metal surface and focus on the surface adsorptive properties.

3.4. TiO_2 Lepidocrocite Supported on Pt and Ag. Among the less common titania polymorphs, lepidocrocite has the interesting feature of being intrinsically bidimensional, consisting of 6 atomic layers.[62] As previously shown, lepidocrocite is the most stable form for an ultrathin titania film,[63] and it has been grown, among others, on Pt(111)[64] and Ag(100) supports.[65] The reducible nature of titania infers a partially negative charge to the film when this is put in contact to a metal support. The smaller the metal's work function, the larger the charge transferred to the TiO_2 film. While in the case of Pt(111) the charge transfer is small, in the case of Ag(100), it is substantial.[41] This has implications on the binding of single adatoms.

As reported in Table 4, the K adatom is always ionized upon adsorption on either free-standing or (Pt, Ag)-supported TiO_2, as clearly shown by the complete quenching of the magnetic moment, the PDOS shown in Figure 4, and the K Bader charge larger than +0.9 lel. The adsorption energy on free-standing TiO_2 (−2.73 eV) is very large compared to the other unsupported oxide films examined so far. This is not surprising, given the reducible nature of titania. On Ag(100), D_e (−2.86 eV) is close to the free-standing case, while it is remarkably larger on Pt(111) (−3.42 eV), in spite of the evidence that the work function in the case of TiO_2/Pt and TiO_2/Ag is quite similar. However, one should consider that the titania film is already negatively charged in the Ag(100) case, which may slightly disfavor the transfer of another electron. K adsorption on titania, moreover, differs from the previously discussed cases under a substantial aspect: when the potassium adatom is ionized, the electron does not reach the metal, but it gets instead trapped on the oxide film, In the case of TiO_2/Pt, the extra electron is trapped on a Ti^{3+} reduced center and a polaron is formed, while on TiO_2/Ag the electron is delocalized over several Ti ions. Also, the strain released on the lepidocrocite film may play a role: while in the case of Ag(100) the film undergoes a large compressive strain along both a (−3.6%) and b (−3.7%) directions, in the case of Pt(111), the strain is compressive along a (−3.1%) and tensile along b (+4.8%). In general, the compressive strain does not help in trapping the electron released by the K adatom upon ionization. The same trend has been observed for the H_2 homolytic dissociation (and subsequent reduction of the TiO_2 support) on Pt- and Ag-supported TiO_2 lepidocrocite, which is also more favorable in the TiO_2/Pt case.[41] The most favorable adsorption site for K is on top of a four-coordinated surface O ion for free-standing and Ag-supported TiO_2 and on top of a surface Ti ion for TiO_2/Pt.

In the case of Pt adsorption, the adatom always maintains a neutral oxidation state. The Pt−O distances are compatible with a covalent bond (slightly above 2 Å). There is, however, a relevant difference in adsorption energy between the free-standing (−3.21 eV) and metal-supported cases (−4.06 eV on TiO_2/Pt and −3.64 eV on TiO_2/Ag). Also, the most stable adsorption site differs from free-standing TiO_2 (on top of a surface Ti ion) compared to the metal-supported TiO_2 (where a lattice site coinciding with a Ti ion from the bottom layer is preferred). It appears, thus, that the metal support plays a role on the Pt_1 adsorption, even though this takes place above the oxide film and no direct contact between the Pt adatom and the metallic support is established.

Au, a definitely more electronegative atom compared to K, remains neutral on free-standing TiO_2, while it acquires a −1 anionic state on Pt- and Ag-supported TiO_2. The tendency of Au adatoms to bind titania in a neutral state is analogous to what was previously reported for the most common TiO_2 surfaces such as rutile(110).[66] In the case of metal-supported titania, the electron is dragged from the metal support to the Au adatom via tunnelling through the film. The ionization of the adatom, as already previously discussed, implies a strong increase in D_e, which passes from −0.39 eV (free-standing TiO_2) to −1.76 eV (TiO_2/Pt) and −1.31 eV (TiO_2/Ag). In spite of a similar work function, TiO_2/Pt binds the Au^- ion stronger than TiO_2/Ag. A possible explanation lies in the fact that in TiO_2/Ag the film is already negatively charged, thus leading to an unfavorable accumulation of negative charges when the Au^- anion is formed.

3.5. ZrO_2 Monolayer Supported on Pt and ZrPt. At variance from bulk ZrO_2, zirconia thin films exhibit a more pronounced reducibility, a fact attributed to the role played by the interaction with the metal support more than to the presence of undercoordinated sites.[42] When K is adsorbed on the free-standing zirconia monolayer, the reduction of the film takes place and the potassium adatom is ionized. As expected, this process is way more favorable in the presence of a metal support where the electron donated from the adatom can spill to.

Indeed, the K adsorption energy is more than double on Pt-supported ZrO_2 (−2.73 eV) and ZrPt-supported ZrO_2 (−2.68

https://dx.doi.org/10.1021/acs.jpcc.0c05958
J. Phys. Chem. C XXXX, XXX, XXX−XXX

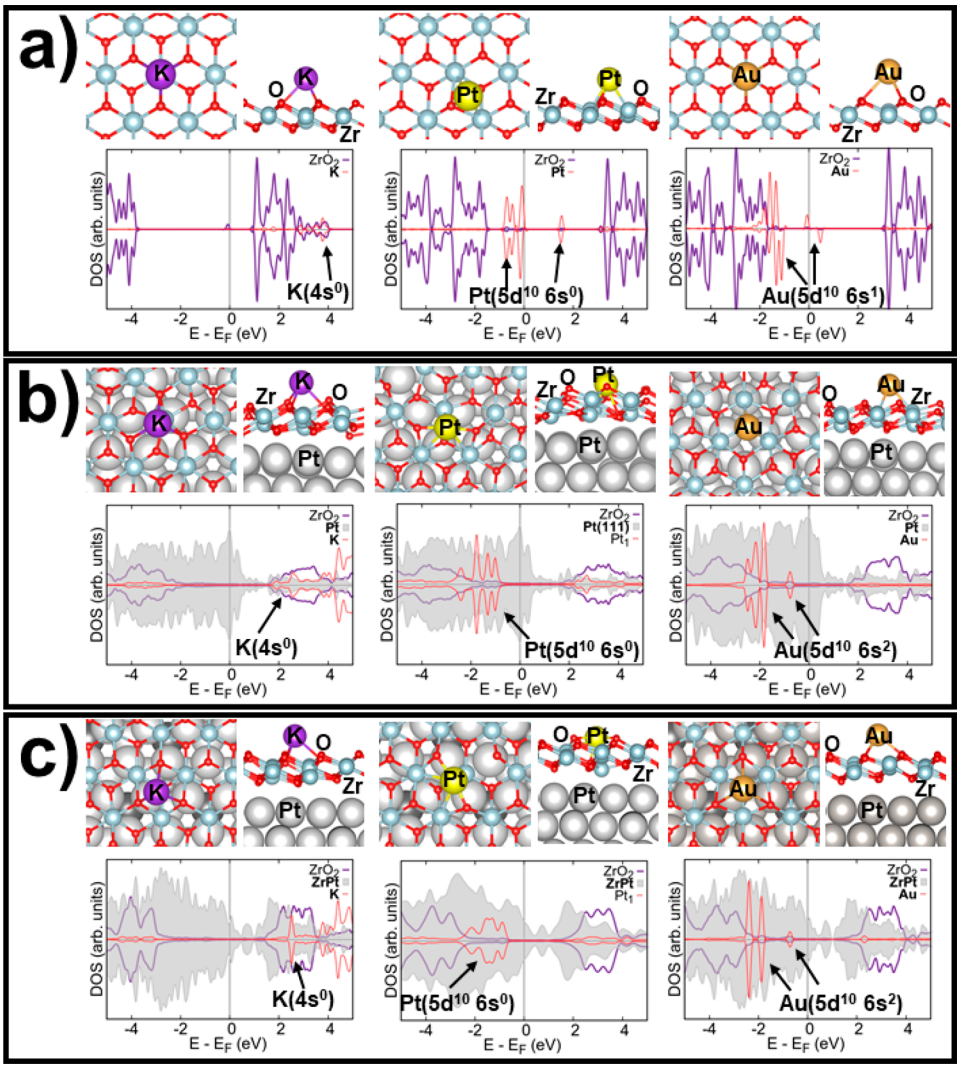

Figure 5. Top view, side view, and PDOS plot of K (left), Pt (middle), and Au (right) adatoms adsorbed on (a) free-standing ZrO_2, (b) ZrO_2/Pt, and (c) ZrO_2/ZrPt.

eV) compared to the free-standing case (−1.04 eV), Table 5. The most stable adsorption site varies from Zr-top (free-standing film) to O-top sites for the metal-supported film. The K−O bond distance is remarkably shorter for metal-supported ZrO_2 compared to the free-standing case, Figure 5.

In analogy to titania films, the Pt adatom maintains a neutral oxidation state on both free-standing and metal-supported ZrO_2. D_e, however, is much smaller on the free-standing film (−2.04 eV) compared to ZrO_2/Pt (−4.41 eV) and ZrO_2/ZrPt (−3.47 eV). A possible explanation of the large difference in D_e between Pt-supported and ZrPt-supported films may lie in the strain released on the film, which is much larger in the case of Pt (+3.5%, Table S2) compared to ZrPt (+1.4%).

As for the Au adatom, in analogy with the case of TiO_2 films, an ionization of the adatom with formation of gold anion is reported on the metal-supported films, while Au remains neutral on free-standing ZrO_2. As expected, a strong increase in adsorption energy is observed upon ionization, passing from −0.44 eV (free-standing ZrO_2) to −1.78 eV (ZrO_2/Pt) and −1.02 eV (ZrO_2/ZrPt). As in the case of Pt, the stronger binding reported on ZrO_2/Pt compared to ZrO_2/ZrPt may be related to the strain.

4. DISCUSSION AND CONCLUSIONS

In this section, we try to summarize and analyze all data exposed previously. In a first attempt to infer a systematic trend to the data set, we start from a simple model based on the charge transfer from/to the adatom as a function of the metal/oxide work function. In principle, one could expect that K will be ionized to K^+ if the Fermi level of the support lies at an energy below (or close to) the adatom's (HOMO). Similarly, a system whose Fermi level lies above the adatom's (LUMO) will act as a potentially strong electron donor. The smaller the work function, thus, the more the system is prone to donate an electron to an electronegative adatom, such as Au; this should be reflected in a larger Au adsorption energy. On the contrary, an electropositive metal atom such as K is expected to be more strongly bound on a film/metal substrate displaying a large work function, i.e., low-lying empty states.

A static picture obtained by simply aligning the oxide/metal Fermi level to the adatom's frontier orbitals, however, would not hold true, since the relaxation of the electronic structure concerns all states from both the substrate and the adatom, affecting also their final reciprocal alignment.[67]

Nevertheless, if the adsorption energy of a potassium adatom is plotted with respect to the substrate's work function, Figure 6,

https://dx.doi.org/10.1021/acs.jpcc.0c05958
J. Phys. Chem. C XXXX, XXX, XXX−XXX

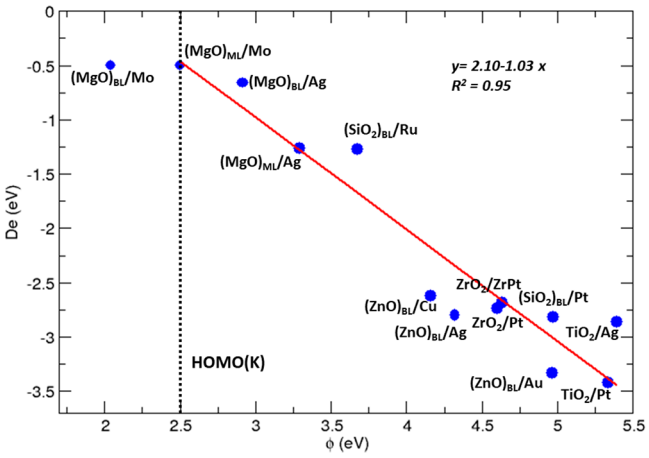

Figure 6. K adsorption energy on all considered systems as a function of the calculated support's work function.

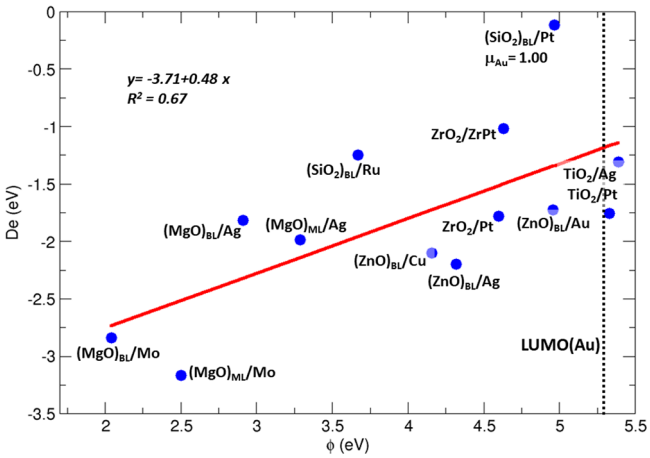

Figure 7. Au adsorption energy on all considered systems as a function of the calculated support's work function.

a rather clear picture emerges. In the case of the Mo-supported MgO bilayer, whose work function is smaller compared to the HOMO of an isolated K adatom, no charge transfer takes place and K is only weakly bound (see section 3.1). The case of $(MgO)_{ML}/Mo$ is intermediate: the Fermi level and the K(HOMO) are at comparable energy, and after the relaxation, the K(4s) orbital is half filled across the Fermi level. Starting from this point, a clear tendency appears, where the K adsorption increases along with the support's work function. In other terms, K adatoms are more strongly adsorbed on systems displaying deeper empty states, in agreement with a simple ionic bond picture. A linear fit along the whole data set (excluding the Mo-supported MgO bilayer, where no charge transfer takes place) yields a good correlation coefficient, R^2 = 0.95. However, other factors play a role beside the respective energy of donor and acceptor states. The ZnO BL supported on coinage metals, for instance, seems to overbind K adatoms compared to other systems, while the SiO_2 BL, on the opposite, binds K less than expected based on the work function argument, just like TiO_2/Ag. The distance between K^+ and the negatively charged metal support may play, in this sense, a role. In the case of $(SiO_2)_{BL}$, for instance, this is particularly large, given the remarkable thickness of the silica bilayer compared to graphitic ZnO. In the case of silver-supported titania, as mentioned in section 3.4, the reducible nature of this oxide plays a relevant role, since the electron is trapped on the oxide film and does not reach the metal. It is thus surprising that the TiO_2/Pt case, where the electron is also trapped on the titania film, lies very close to a trend line relative to mostly non-reducible oxides. This fact, however, can also be fortuitous.

In the case of Au, one would expect a specular behavior compared to K, i.e., a stronger bonding on systems displaying a small work function (i.e., relatively shallow donor states). While looking at Figure 7, one can notice that (i) the Au(LUMO) lies at an energy lower or comparable to that of the Fermi level of all systems, including those displaying the larger work function in the whole set, like TiO_2/Pt and TiO_2/Ag, and (ii) the overall agreement with the simple ionic-bond picture is much worse compared to the case of potassium, even though a decreasing trend in bond strength as a function of φ is still evident.

The charging of Au, for instance, does not take place in the case of $(SiO_2)_{BL}$/Pt, in spite of a smaller work function compared to TiO_2/Ag and TiO_2/Pt. Also, the difference in D_e between TiO_2/Ag and TiO_2/Pt is quite large, if one considers that these two systems display the same chemical nature of the film and very similar work functions. One can only stress once more how other factors can play a role beyond the support's work function.[67] The silica bilayer, for instance, displays smaller Au adsorption energies compared to what one would expect, just like in the case of potassium. This seems to strengthen the observation that the large distance from the metal substrate may play a role, for both negatively and positively charged adsorbates. Also, the smaller D_e observed for $(MgO)_{BL}$/Ag compared to $(MgO)_{ML}$/Ag and $(MgO)_{BL}$/Mo compared to $(MgO)_{ML}$/Mo seems to go in this direction, given that BLs keep the adatom more distant from the metal support compared to MLs. This may result in a weaker interaction between the charged adatom and the image charge that forms in a metallic conductor when electrons polarize in response to the presence of a charge.

The overlap between the Au orbitals and those from the metal support may also explain why the Au adatom is more strongly adsorbed on ZnO/Ag compared to ZnO/Cu.

Finally, as discussed in section 3, one should also consider that the strain and local geometric relaxations, not always easy to quantify, may influence the complexation capability of the oxide film.

The case of platinum radically differs from potassium and gold. Here, the interaction established between the adatom and the oxide film has in most cases a predominantly covalent polar nature. As shown in Figure 8, there is no correlation whatsoever between the support's work function and the adsorption energy, as the bonding does not have charge transfer character.

We have also tried to correlate D_e with the shortest Pt−O distance (Figure 9). The platinum single atom, in fact, may bind an oxide surface in several ways, interacting with both oxygen and metal ions. The overlap with the orbitals of the underlying metal surface also plays a role. As shown in Figure 8, the oxidation state of Pt varies from 0 to −2 depending on the substrate. The $(Pt)^{2-}$ species is observed on $(MgO)_{ML}$/Mo, where the proximity to the electropositive molybdenum surface allows for a double charge transfer, resulting in a strong ionic bond. Similarly, also in the case of ZnO/Ag, Pt acquires a −2 oxidation state. One can notice from Figure 9 how this influences the bonding geometry of the adatom, evidencing the strong repulsion with oxygen ions from the oxide. One can notice a general trend correlating the Pt oxidation state to the Pt−O distance where, as one could expect, larger Pt−O distances are observed for more negatively charged Pt adatoms.

https://dx.doi.org/10.1021/acs.jpcc.0c05958
J. Phys. Chem. C XXXX, XXX, XXX−XXX

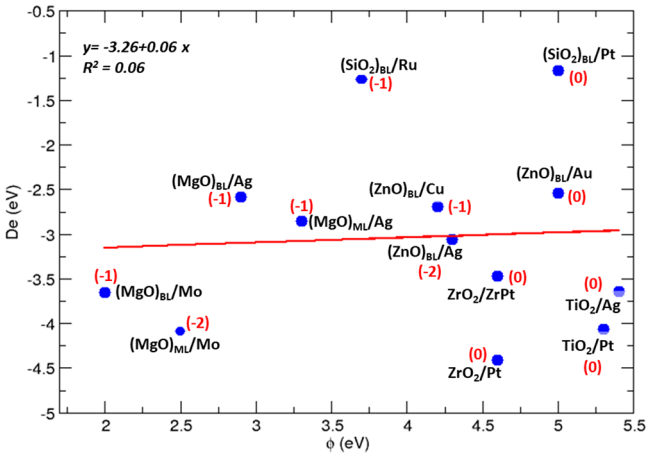

Figure 8. Pt adsorption energy on all considered systems as a function of the calculated supported film's work function. The Pt oxidation state is reported in parentheses.

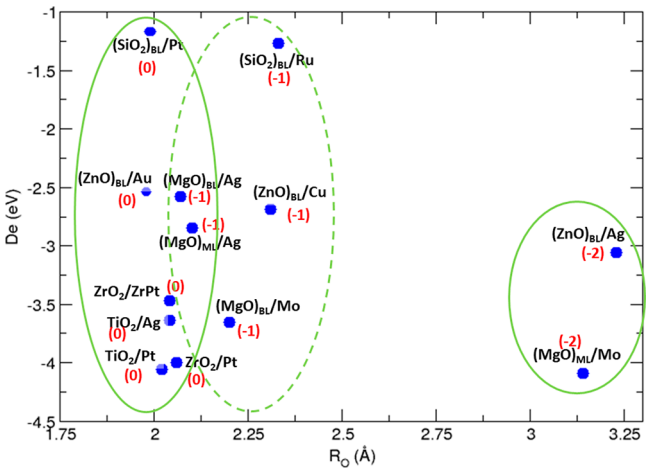

Figure 9. Pt adsorption energy on all considered systems as a function of the minimum Pt−O distance. The Pt oxidation state is reported in parentheses.

However, the Pt oxidation state does not correlate with the adsorption energy.

In general, a stiff and rigid film such as the SiO_2 BL seems to interact weakly with the Pt atom. On the contrary, flexible structures like the ZrO_2 ML, prone to a pronounced reconstruction upon adsorption of the Pt adatom, ensure a strong bond. The lepidocrocite TiO_2 film is also a very favorable adsorption substrate for Pt, thanks to its structure providing cavities where the adatom is bound by several surrounding atoms. The trend in D_e for Pt_1 on ZnO BL supported on coinage metals is, however, a bit elusive: while it seems clear why the Pt adatom remains neutral on most electronegative metal supports of the series (Au) and acquires a −1 charge on ZnO/Cu, it is not easy to explain why the adsorption energy (and the charge transferred to Pt) on ZnO/Ag is remarkably larger than that on ZnO/Cu.

In conclusion, this work has been driven by the idea of performing a systematic study on the surface chemical properties of a peculiar class of materials, the oxide thin films supported on metals. To this end, we have simulated the adsorption of the simplest chemical entities, the single atoms. We have chosen a strong electron donor (K), a very electronegative metal (Au), and a transition metal atom more prone to establish covalent interactions (Pt). The goal was to unravel the role of the metal/oxide interplay in driving the surface chemistry of these materials. In the case of K and, to a less extent, Au, the work function of the metal/oxide substrate is the key parameter in determining the bonding strength of the adatom: potassium is ionized to K^+ in most cases, and the ionic bond which is then established is stronger the deeper the acceptor states of the substrate. Similarly, the strong tendency of Au single atoms to form Au^- anions implies a stronger bond on systems with a small work function, i.e., with occupied states at relative high energy. However, this barely electrostatic picture is complicated by the presence of other important factors, such as the film's thickness (and, in general, the distance from the metal support), the more or less diffuse nature of the metal orbitals, the surface morphology, and the oxide's reducibility.

The case of Pt represents a more complicated picture, where the physical properties of the substrate such as the work function play a little role. In general, the covalent−polar nature of the platinum−oxide interaction leads to strong bonds on films where the adatom can be efficiently complexed. However, a very large charge transfer toward the Pt adatom has been observed in few cases.

Finally, it is worth mentioning a delicate methodological aspect: through all of this work, the oxidation state of the adatom has been determined by carefully looking at its density of states and magnetic moment. As one can see through the whole section 3, even though the Bader model is physically well grounded, the charges are often inaccurate (for the Au anion in particular), and an assignment based on Bader charges only could lead to misleading conclusions. We can thus only warn against the tendency in the computational chemistry community to rely too much on any sort of charge partition scheme.

■ ASSOCIATED CONTENT

Supporting Information

The Supporting Information is available free of charge at https://pubs.acs.org/doi/10.1021/acs.jpcc.0c05958.

List of adopted pseudopotentials and list of all metal/oxide supercells adopted in this work (complete list of all local minima not considered in the discussion) (PDF)

■ AUTHOR INFORMATION

Corresponding Author

Sergio Tosoni − *Dipartimento di Scienza dei Materiali, Università di Milano-Bicocca, 20125 Milano, Italy;* orcid.org/0000-0001-5700-4086; Phone: +39-02-64485214; Email: sergio.tosoni@unimib.it

Author

Gianfranco Pacchioni − *Dipartimento di Scienza dei Materiali, Università di Milano-Bicocca, 20125 Milano, Italy;* orcid.org/0000-0002-4749-0751

Complete contact information is available at: https://pubs.acs.org/10.1021/acs.jpcc.0c05958

Notes

The authors declare no competing financial interest.

■ ACKNOWLEDGMENTS

Financial support from the Italian Ministry of University and Research (MIUR) through PRIN Project 20179337R7MULTI-e "Multielectron transfer for the conversion of small molecules:

https://dx.doi.org/10.1021/acs.jpcc.0c05958
J. Phys. Chem. C XXXX, XXX, XXX−XXX

an enabling technology for the chemical use of renewable energy" and the grant Dipartimenti di Eccellenza -2017 "Materials For Energy" is gratefully acknowledged. We acknowledge CINECA under the ISCRAB initiatives for the availability of high performance computing resources and support.

REFERENCES

(1) Xu, X.; Goodman, D. W. New Approach to the Preparation of Ultrathin Silicon Dioxide Films at Low Temperatures. *Appl. Phys. Lett.* **1992**, *61*, 774−776.
(2) Freund, H.-J.; Kuhlenbeck, H.; Staemmler, V. Oxide Surfaces. *Rep. Prog. Phys.* **1996**, *59*, 283.
(3) Freund, H. J.; Pacchioni, G. Oxide Ultra-Thin Films on Metals: New Materials for the Design of Supported Metal Catalysts. *Chem. Soc. Rev.* **2008**, *37*, 2224−2242.
(4) *Oxide Ultrathin Films: Science and Technology*; Pacchioni, G., Valeri, S., Eds.; Wiley-VCH: Weinheim, Germany, 2012.
(5) Giordano, L.; Pacchioni, G. Oxide Films at the Nanoscale: New Structures, New Functions, and New Materials. *Acc. Chem. Res.* **2011**, *44*, 1244−1252.
(6) Parkin, S. S. P.; Kaiser, C.; Panchula, A.; Rice, P. M.; Hughes, B.; Samant, M.; Yang, S. H. Giant Tunnelling Magnetoresistance at Room Temperature with MgO (100) Tunnel Barriers. *Nat. Mater.* **2004**, *3*, 862−867.
(7) Song, Z.; Zhao, B.; Xu, H.; Cheng, P. Remarkably Strong Chemisorption of Nitric Oxide on Insulating Oxide Films Promoted by Hybrid Structure. *J. Phys. Chem. C* **2017**, *121*, 21482−21490.
(8) Fortunato, E.; Barquinha, P.; Martins, R. Oxide Semiconductor Thin-Film Transistors: A Review of Recent Advances. *Adv. Mater.* **2012**, *24*, 2945−2986.
(9) Nilius, N. Properties of Oxide Thin Films and Their Adsorption Behavior Studied by Scanning Tunneling Microscopy and Conductance Spectroscopy. *Surf. Sci. Rep.* **2009**, *64*, 595−659.
(10) Pacchioni, G.; Giordano, L.; Baistrocchi, M. Charging of Metal Atoms on Ultrathin MgO/Mo(100) Films. *Phys. Rev. Lett.* **2005**, *94*, 226104.
(11) Giordano, L.; Baistrocchi, M.; Pacchioni, G. Bonding of Pd, Ag, and Au Atoms on MgO(100) Surfaces and MgO/Mo(100) Ultra-Thin Films: A Comparative DFT Study. *Phys. Rev. B: Condens. Matter Mater. Phys.* **2005**, *72*, 115403.
(12) Sterrer, M.; Risse, T.; Martinez Pozzoni, U.; Giordano, L.; Heyde, M.; Rust, H. P.; Pacchioni, G.; Freund, H. J. Control of the Charge State of Metal Atoms on Thin MgO Films. *Phys. Rev. Lett.* **2007**, *98*, 096107.
(13) Gonchar, A.; Risse, T.; Freund, H.-J.; Giordano, L.; Di Valentin, C.; Pacchioni, G. Activation of Oxygen on MgO: O2.- Radical Ion Formation on Thin, Metal-Supported MgO(001) Films. *Angew. Chem., Int. Ed.* **2011**, *50*, 2635−2638.
(14) Grönbeck, H. Mechanism for NO2 Charging on Metal Supported MgO. *J. Phys. Chem. B* **2006**, *110*, 11977−11981.
(15) Starr, D. E.; Weis, C.; Yamamoto, S.; Nilsson, A.; Bluhm, H. NO 2 Adsorption on Ag(100) Supported MgO(100) Thin Films: Controlling the Adsorption State with Film Thickness. *J. Phys. Chem. C* **2009**, *113*, 7355−7363.
(16) Tosoni, S.; Spinnato, D.; Pacchioni, G. DFT Study of CO2 Activation on Doped and Ultrathin MgO Films. *J. Phys. Chem. C* **2015**, *119*, 27594−27602.
(17) Ricci, D.; Bongiorno, A.; Pacchioni, G.; Landman, U. Bonding Trends and Dimensionality Crossover of Gold Nanoclusters on Metal-Supported MgO Thin Films. *Phys. Rev. Lett.* **2006**, *97*, 036106.
(18) Simic-Milosevic, V.; Heyde, M.; Lin, X.; König, T.; Rust, H. P.; Sterrer, M.; Risse, T.; Nilius, N.; Freund, H. J.; Giordano, L.; et al. Charge-Induced Formation of Linear Au Clusters on Thin MgO Films: Scanning Tunneling Microscopy and Density-Functional Theory Study. *Phys. Rev. B: Condens. Matter Mater. Phys.* **2008**, *78*, 235429.
(19) Calaza, F.; Stiehler, C.; Fujimori, Y.; Sterrer, M.; Beeg, S.; Ruiz-Oses, M.; Nilius, N.; Heyde, M.; Parviainen, T.; Honkala, K.; et al. Carbon Dioxide Activation and Reaction Induced by Electron Transfer at an Oxide-Metal Interface. *Angew. Chem., Int. Ed.* **2015**, *54*, 12484−12487.
(20) Cipriano, L. A.; Tosoni, S.; Pacchioni, G. CH3Br Adsorption on MgO/Mo Ultrathin Films: A DFT Study. *Surf. Sci.* **2018**, *672*, 1−6.
(21) Hurdax, P.; Hollerer, M.; Puschnig, P.; Lüftner, D.; Egger, L.; Ramsey, M. G.; Sterrer, M. Controlling the Charge Transfer across Thin Dielectric Interlayers. *Adv. Mater. Interfaces* **2020**, *7*, 2000592.
(22) Naumann d'Alnoncourt, R.; Kurtz, M.; Wilmer, H.; Löffler, E.; Hagen, V.; Shen, J.; Muhler, M. The Influence of ZnO on the Differential Heat of Adsorption of CO on Cu Catalysts: A Microcalorimetric Study. *J. Catal.* **2003**, *220*, 249−253.
(23) Naumann D'Alnoncourt, R.; Xia, X.; Strunk, J.; Löffler, E.; Hinrichsen, O.; Muhler, M. The Influence of Strongly Reducing Conditions on Strong Metal-Support Interactions in Cu/ZnO Catalysts Used for Methanol Synthesis. *Phys. Chem. Chem. Phys.* **2006**, *8*, 1525−1538.
(24) Schott, V.; Oberhofer, H.; Birkner, A.; Xu, M.; Wang, Y.; Muhler, M.; Reuter, K.; Wöll, C. Chemical Activity of Thin Oxide Layers: Strong Interactions with the Support Yield a New Thin-Film Phase of Zno. *Angew. Chem., Int. Ed.* **2013**, *52*, 11925−11929.
(25) Tosoni, S.; Li, C.; Schlexer, P.; Pacchioni, G. CO Adsorption on Graphite-like ZnO Bilayers Supported on Cu(111), Ag(111), and Au(111) Surfaces. *J. Phys. Chem. C* **2017**, *121*, 27453−27461.
(26) Thang, H. V.; Tosoni, S.; Pacchioni, G. Evidence of Charge Transfer to Atomic and Molecular Adsorbates on ZnO/X(111) (X = Cu, Ag, Au) Ultrathin Films. Relevance for Cu/ZnO Catalysts. *ACS Catal.* **2018**, *8*, 4110−4119.
(27) Thang, H. V.; Pacchioni, G. Spontaneous Formation of Gold Cluster Anions on ZnO/Cu(111) Bilayer Films. *J. Phys. Chem. C* **2019**, *123*, 7644−7653.
(28) DeRita, L.; Resasco, J.; Dai, S.; Boubnov, A.; Thang, H. V.; Hoffman, A. S.; Ro, I.; Graham, G. W.; Bare, S. R.; Pacchioni, G.; et al. Structural Evolution of Atomically Dispersed Pt Catalysts Dictates Reactivity. *Nat. Mater.* **2019**, *18*, 746−751.
(29) Wang, H.; Xu, D.; Guan, E.; Wang, L.; Zhang, J.; Wang, C.; Wang, S.; Xu, H.; Meng, X.; Yang, B.; et al. Atomically Dispersed Ru on Manganese Oxide Catalyst Boosts Oxidative Cyanation. *ACS Catal.* **2020**, *10*, 6299−6308.
(30) Qiao, B.; Wang, A.; Yang, X.; Allard, L. F.; Jiang, Z.; Cui, Y.; Liu, J.; Li, J.; Zhang, T. Single-Atom Catalysis of CO Oxidation Using Pt1/FeOx. *Nat. Chem.* **2011**, *3*, 634−641.
(31) Lin, J.; Qiao, B.; Li, N.; Li, L.; Sun, X.; Liu, J.; Wang, X.; Zhang, T. Little Do More: A Highly Effective Pt_1/FeO_x Single-Atom Catalyst for the Reduction of NO by H_2. *Chem. Commun.* **2015**, *51*, 7911−7914.
(32) Wang, L.; Chen, W.; Zhang, D.; Du, Y.; Amal, R.; Qiao, S.; Wu, J.; Yin, Z. Surface Strategies for Catalytic CO_2 Reduction: From Two-Dimensional Materials to Nanoclusters to Single Atoms. *Chem. Soc. Rev.* **2019**, *48*, 5310−5349.
(33) Baumann, S.; Donati, F.; Stepanow, S.; Rusponi, S.; Paul, W.; Gangopadhyay, S.; Rau, I. G.; Pacchioni, G. E.; Gragnaniello, L.; Pivetta, M.; et al. Origin of Perpendicular Magnetic Anisotropy and Large Orbital Moment in Fe Atoms on MgO. *Phys. Rev. Lett.* **2015**, *115*, 237202.
(34) Donati, F.; Rusponi, S.; Stepanow, S.; Wäckerlin, C.; Singha, A.; Persichetti, L.; Baltic, R.; Diller, K.; Patthey, F.; Fernandes, E.; et al. Magnetic Remanence in Single Atoms. *Science* **2016**, *352*, 318−321.
(35) Fernandes, E.; Donati, F.; Patthey, F.; Stavrić, S.; Šljivančanin, Ž.; Brune, H. Adsorption Sites of Individual Metal Atoms on Ultrathin MgO(100) Films. *Phys. Rev. B: Condens. Matter Mater. Phys.* **2017**, *96*, 045419.
(36) Yang, K.; Paul, W.; Phark, S. H.; Willke, P.; Bae, Y.; Choi, T.; Esat, T.; Ardavan, A.; Heinrich, A. J.; Lutz, C. P. Coherent Spin Manipulation of Individual Atoms on a Surface. *Science* **2019**, *366*, 509−512.
(37) Savio, L.; Smerieri, M.; Vattuone, L.; Tosoni, S.; Pacchioni, G.; Rocca, M. Interface Oxygen Induced Internal Structures of Ultrathin MgO Islands Grown on Ag(100). *J. Phys. Chem. C* **2020**, *124*, 8834−8842.
(38) Pal, J.; Smerieri, M.; Celasco, E.; Savio, L.; Vattuone, L.; Ferrando, R.; Tosoni, S.; Giordano, L.; Pacchioni, G.; Rocca, M. How

https://dx.doi.org/10.1021/acs.jpcc.0c05958
J. Phys. Chem. C XXXX, XXX, XXX−XXX

Growing Conditions and Interfacial Oxygen Affect the Final Morphology of MgO/Ag(100) Films. *J. Phys. Chem. C* **2014**, *118*, 26091−26102.
(39) Pacchioni, G.; Freund, H. Electron Transfer at Oxide Surfaces. the MgO Paradigm: From Defects to Ultrathin Films. *Chem. Rev.* **2013**, *113*, 4035−4072.
(40) Lewandowski, A. L.; Schlexer, P.; Tosoni, S.; Gura, L.; Marschalik, P.; Buchner, C.; Burrall, H.; Burson, K. M.; Schneider, W.-D.; Pacchioni, G.; et al. Determination of Silica and Germania Film Network Structures on Ru(0001) at the Atomic Scale. *J. Phys. Chem. C* **2019**, *123*, 7889−7897.
(41) Tosoni, S.; Pacchioni, G. Hydrogen Adsorption on Free-Standing and Ag-Pt Supported TiO2 Thin Films. *J. Phys. Chem. C* **2019**, *123*, 7952−7960.
(42) Ruiz Puigdollers, A.; Pacchioni, G. Reducibility of ZrO2/Pt3Zr and ZrO2/Pt 2D Films Compared to Bulk Zirconia: A DFT+U Study of Oxygen Removal and H2 Adsorption. *Nanoscale* **2017**, *9*, 6866−6876.
(43) Martinez, U.; Giordano, L.; Pacchioni, G. Tuning the Work Function of Ultrathin Oxide Films on Metals by Adsorption of Alkali Atoms. *J. Chem. Phys.* **2008**, *128*, 164707.
(44) Schlexer, P.; Giordano, L.; Pacchioni, G. Adsorption of Li, Na, K, and Mg Atoms on Amorphous and Crystalline Silica Bilayers on Ru(0001): A DFT Study. *J. Phys. Chem. C* **2014**, *118*, 15884−15891.
(45) Büchner, C.; Lichtenstein, L.; Stuckenholz, S.; Heyde, M.; Ringleb, F.; Sterrer, M.; Kaden, W. E.; Giordano, L.; Pacchioni, G.; Freund, H. J. Adsorption of Au and Pd on Ruthenium-Supported Bilayer Silica. *J. Phys. Chem. C* **2014**, *118*, 20959−20969.
(46) Choi, J. I. J.; Mayr-Schmölzer, W.; Valenti, I.; Luches, P.; Mittendorfer, F.; Redinger, J.; Diebold, U.; Schmid, M. Metal Adatoms and Clusters on Ultrathin Zirconia Films. *J. Phys. Chem. C* **2016**, *120*, 9920−9932.
(47) Kresse, G.; Furthmüller, J. Efficiency of Ab-Initio Total Energy Calculations for Metals and Semiconductors Using a Plane-Wave Basis Set. *Comput. Mater. Sci.* **1996**, *6*, 15−50.
(48) Kresse, G.; Furthmüller, J. Efficient Iterative Schemes for *Ab Initio* Total-Energy Calculations Using a Plane-Wave Basis Set. *Phys. Rev. B: Condens. Matter Mater. Phys.* **1996**, *54*, 11169−11186.
(49) Blöchl, P. E. Projector Augmented-Wave Method. *Phys. Rev. B: Condens. Matter Mater. Phys.* **1994**, *50*, 17953−17979.
(50) Kresse, G.; Joubert, D. From Ultrasoft Pseudopotentials to the Projector Augmented-Wave Method. *Phys. Rev. B: Condens. Matter Mater. Phys.* **1999**, *59*, 1758−1775.
(51) Perdew, J. P.; Burke, K.; Ernzerhof, M. Generalized Gradient Approximation Made Simple. *Phys. Rev. Lett.* **1996**, *77*, 3865−3868.
(52) Anisimov, V. I.; Zaanen, J.; Andersen, O. K. Band Theory and Mott Insulators: Hubbard U Instead of Stoner I. *Phys. Rev. B: Condens. Matter Mater. Phys.* **1991**, *44*, 943−954.
(53) Dudarev, S.; Botton, G. Electron-Energy-Loss Spectra and the Structural Stability of Nickel Oxide: An LSDA+U Study. *Phys. Rev. B: Condens. Matter Mater. Phys.* **1998**, *57*, 1505−1509.
(54) Capdevila-Cortada, M.; Łodziana, Z.; López, N. Performance of DFT+U Approaches in the Study of Catalytic Materials. *ACS Catal.* **2016**, *6*, 8370−8379.
(55) Prada, S.; Giordano, L.; Pacchioni, G.; Noguera, C.; Goniakowski, J. Properties of Pt-Supported Iron Oxide Ultra-Thin Films: Similarity of Hubbard-Corrected and Hybrid Density Functional Theory Description. *J. Chem. Phys.* **2014**, *141*, 144702.
(56) Prada, S.; Giordano, L.; Pacchioni, G.; Goniakowski, J. Theoretical Description of Metal/Oxide Interfacial Properties: The Case of MgO/Ag(001). *Appl. Surf. Sci.* **2016**, *390*, 578−582.
(57) Grimme, S. Semiempirical GGA-Type Density Functional Constructed with a Long-Range Dispersion Correction. *J. Comput. Chem.* **2006**, *27*, 1787−1799.
(58) Tosoni, S.; Sauer, J. Accurate Quantum Chemical Energies for the Interaction of Hydrocarbons with Oxide Surfaces: CH4/MgO(001). *Phys. Chem. Chem. Phys.* **2010**, *12*, 14330−14340.
(59) Bader, R. F. W. A Quantum Theory of Molecular Structure and Its Applications. *Chem. Rev.* **1991**, *91*, 893−928.
(60) Henkelman, G.; Arnaldsson, A.; Jónsson, H. A Fast and Robust Algorithm for Bader Decomposition of Charge Density. *Comput. Mater. Sci.* **2006**, *36*, 354−360.
(61) Chiesa, M.; Giamello, E.; Di Valentin, C.; Pacchioni, G.; Sojka, Z.; Van Doorslaer, S. Nature of the Chemical Bond between Metal Atoms and Oxide Surfaces: New Evidences from Spin Density Studies of K Atoms on Alkaline Earth Oxides. *J. Am. Chem. Soc.* **2005**, *127*, 16935−16944.
(62) De Angelis, F.; Di Valentin, C.; Fantacci, S.; Vittadini, A.; Selloni, A. Theoretical Studies on Anatase and Less Common TiO 2 Phases: Bulk, Surfaces, and Nanomaterials. *Chem. Rev.* **2014**, *114*, 9708−9753.
(63) Vittadini, A.; Casarin, M. Ab Initio Modeling of TiO2 Nanosheets. *Theor. Chem. Acc.* **2008**, *120*, 551−556.
(64) Zhang, Y.; Giordano, L.; Pacchioni, G.; Vittadini, A.; Sedona, F.; Finetti, P.; Granozzi, G. The Structure of a Stoichiometric TiO2 Nanophase on Pt(1 1 1). *Surf. Sci.* **2007**, *601*, 3488−3496.
(65) Atrei, A.; Ferrari, A. M.; Szieberth, D.; Cortigiani, B.; Rovida, G. Lepidocrocite-like Structure of the TiO2Monolayer Grown on Ag(100). *Phys. Chem. Chem. Phys.* **2010**, *12*, 11587−11595.
(66) Tosoni, S.; Pacchioni, G. Trends in Adhesion Energies of Gold on MgO(100), Rutile TiO2(110), and CeO2(111) Surfaces: A Comparative DFT Study. *J. Phys. Chem. C* **2017**, *121*, 28328−28338.
(67) Prada, S.; Martinez, U.; Pacchioni, G. Work Function Changes Induced by Deposition of Ultrathin Dielectric Films on Metals: A Theoretical Analysis. *Phys. Rev. B: Condens. Matter Mater. Phys.* **2008**, *78*, 235423.

https://dx.doi.org/10.1021/acs.jpcc.0c05958
J. Phys. Chem. C XXXX, XXX, XXX−XXX